ARTICLES

Journal of Semiconductors
(2022) 43, 032001
doi: 10.1088/1674-4926/43/3/032001

Fe^{3+}-substitution effect on the thermal variation of *J–E* characteristics and DC resistivity of quadruple perovskite $CaCu_3Ti_4O_{12}$

Kunal B. Modi[1, †], Pooja Y. Raval[2], Dolly J. Parekh[1], Shrey K. Modi[3], Niketa P. Joshi[1], Akshay R. Makadiya[1], Nimish H. Vasoya[4], and Utpal S. Joshi[5]

[1]Department of Physics, Saurashtra University, Rajkot 360005, India

[2]Department of Physics, C. U. Shah University, Wadhwan City, Surendranagar 363030, India

[3]Department of Environment Engineering, L. D. Engineering College, Ahmedabad 380015, India

[4]Department of Balbhavan, Children´s University, Sector – 20, Gandhinagar 382015, India

[5]Department of Physics, University School of Sciences, Gujarat University, Ahmedabad 380009, India

Abstract: The electrical properties of cubic perovskite series, $CaCu_{3-x}Ti_{4-x}Fe_{2x}O_{12}$ with x = 0.0, 0.1, 0.3, 0.5, and 0.7, have been studied by employing current density as a function of electric field characteristics registered at different temperatures and thermal variations of direct current electrical resistivity measurements. All of the compositions exhibit strong non-ohmic behavior. The concentration dependence of breakdown field, the temperature at which switching action takes place, and maximum value of current density (J_{max}) has been explained on account of structural, microstructural, and positron lifetime parameters. The highest ever reported value of J_{max} = 327 mA/cm^2 has been observed for pristine composition. The values of the nonlinear coefficient advise the suitability of ceramics for low-voltage varistor applications. The Arrhenius plots show typical semiconducting nature. The activation energy values indicate that electric conduction proceeds through electrons with deformation in the system.

Key words: perovskites; magnetic materials; *J–E* characteristics; capacitor

Citation: K B Modi, P Y Raval, D J Parekh, S K Modi, N P Joshi, A R Makadiya, N H Vasoya, and U S Joshi, Fe^{3+}-substitution effect on the thermal variation of *J– E* characteristics and DC resistivity of quadruple perovskite $CaCu_3Ti_4O_{12}$[J]. *J. Semicond.*, 2022, 43(3), 032001. https://doi.org/10.1088/1674-4926/43/3/032001

1. Introduction

In 2000, Subramanian *et al.*[1] and Ramirez *et al.*[2] noticed that the dielectric permittivity (ε') of a microcrystalline sample of perovskite derivative calcium-copper-titanate ($CaCu_3Ti_4O_{12}$) abruptly jumps by a factor of 100 when heated above T = 90 K (at 1 kHz frequency). This material at T = 100 K exhibits a huge value of ε' of the order of 10^4 and ε' becomes weakly dependent on temperature for T = 100–320 K. These unusual and fascinating properties make them suitable for potent applications, such as in multilayer ceramic capacitors, devices for memory and high-density energy storage[3]. In 2003, Kretly *et al.*[4] successfully used $CaCu_3Ti_4O_{12}$ substrates for microwave devices and antennas. In 2004, Chung *et al.*[5] observed highly non-ohmic current–voltage characteristics in $CaCu_3Ti_4O_{12}$ with nonlinear coefficient ≈ 912. This leads to the use of this material as an efficient switching (varistor-type device) and gas sensing device. In 2012, Felix *et al.*[6] investigated thin films of $CaCu_3Ti_4O_{12}$ for potential applications, such as gas sensing, rectification, and resistive switching. In 2016, it was demonstrated that this material could serve as photocatalytic and photoelectrochemical materials with an excellent performance in visible light[7]. Since then, pure and substituted $CaCu_3Ti_4O_{12}$ and related materials in monocrystalline, microcrystalline, nanophasic, nanocomposites, and thin-film forms have been extensively researched for potential use in a wide range of applications. In 2020, Chhetry *et al.*[8] revealed a novel possibility for the easy design and development of superior $CaCu_3Ti_4O_{12}$ based capacitive sensors with versatile characteristics. Chattopadhyay *et al.*[9] suggested the possible use of $CaCu_3Ti_4O_{12}$ nanopowder for application in a humidity sensor. Many research reports describing the fundamentals of experimental and theoretical researches on $CaCu_3Ti_4O_{12}$ based ceramic materials are available in the literature.

Varistors are voltage-dependent resistors that demonstrate strong nonlinear current versus voltage (*I–V*) characteristics. The electrical properties of varistors are chiefly influenced by grain-boundary interface states. The principal function of a varistor is to sense and control transient voltage surges. When a varistor is subjected to a high applied voltage, its impedance changes from a near open circuit to a highly conducting state, which results in the clamping of the transient voltage to a safe level and thus electronic components of high-cost electronic devices may be protected. Between 2016 and 2021, a limited number of research reports were published on *J–E* characteristics of $CaCu_3Ti_4O_{12}$ cubic perovskites substituted with different metallic cation/cations. For example, the nonlinear electrical properties with high-performance dielectric behavior of $CaCu_{2.95}Cr_{0.05}Ti_{4.1}$

Correspondence to: K B Modi, kunalbmodi2003@yahoo.com
Received 15 SEPTEMBER 2021; Revised 19 NOVEMBER 2021.

O_{12} have been studied by Prompa *et al.*[10]. The improvement of the breakdown field and the dielectric properties of Bi^{3+}-Al^{3+} co-doped $CaCu_3Ti_4O_{12}$ have been investigated by Ren *et al.*[11]. The dielectric properties, nonlinear electrical response, and microstructural evolution of $CaCu_3Ti_{4-x}Sn_xO_{12}$ ceramics prepared by a double ball-milling process have been investigated by Boonlakhorn *et al.*[12]. Cortes *et al.*[13] performed dielectric and non-ohmic properties of $Ca_2Cu_2Ti_{4-x}Sn_xO_{12}$ multiphasic ceramic composites. Comparative studies on pure and Sr^{2+} and Ni^{2+} doped and co-doped ceramics with special emphasis on the enhancement of dielectric properties have been published by Rhouma *et al.*[14]. Wu *et al.*[15] accomplished the effect of Ba^{2+} substitution on microstructure and electrical properties of $Ca_{1-x}Ba_xCu_3Ti_4O_{12}$ ceramics. Enhanced nonlinear *I*–*V* response of Te^{4+} substituted $CaCu_3Ti_4O_{12}$ ceramics has been studied by Barman *et al.*[16]. Meanwhile, the improvement in varistor properties of aliovalent Cr^{3+} substitution for Ti^{4+} in $CaCu_3Ti_{4-x}Cr_xO_{12-\delta}$ series has been investigated by Grezebielucka *et al.*[17]. Sun *et al.* studied improved dielectric properties of In^{3+} and Ta^{4+} co-substituted $CaCu_3Ti_4O_{12}$ ceramics prepared by spark plasma sintering[18]. Very high-performance dielectric and non-ohmic properties of X and R-type $Ca_{1-1.5x}Ho_xCu_3Ti_4O_{12}/TiO_2$ ceramics have been investigated by Sriakdee *et al.*[19]. Finally, enhanced giant dielectric properties and improved electrical response in acceptor–donner (Al and Ta)-substituted $CaCu_3Ti_4O_{12}$ polycrystalline ceramics have been carried out by Boonlakhorn *et al.*[20]. Unfortunately, these studies carry very limited and similar information, and were performed at T = 300 K. The same is the case with the thermal variation of dc electrical resistivity, ρ_{dc} (T), study. To the best of our knowledge, only a handful of research articles describing ρ_{dc} (T) characteristics of bulk[21–24] and thin films[25] of $CaCu_3Ti_4O_{12}$ are available in the literature. This gap has motivated us to carry out a systematic study of current density versus electric field characteristics over a wide temperature range and thermal variation of dc resistivity study of polycrystalline samples of quadruple perovskite series, $CaCu_{3-x}Ti_{4-x}Fe_{2x}O_{12}$ with x = 0.0, 0.1, 0.3, 0.5, and 0.7.

Based on the following facts, the work presented in this communication is important as well as different from the existing literature. The electrical properties, *J*–*E* characteristics and dc resistivity of $CaCu_{3-x}Ti_{4-x}Fe_{2x}O_{12}$ with x = 0.0, 0.1, 0.3, 0.5, and 0.7 have been studied over a wide temperature range of T = 313 to 773 K as a function of Fe-concentration (x). The compositional variation of various electrical parameters (e.g., maximum current density, breakdown electric field, the temperature at which switching action takes place, Schottky barrier height, non-linearity coefficient, and activation energy) are determined and correlated with structural parameters (i.e., lattice constant, cationic distribution), microstructural parameters (i.e., grain size, microstrain, dislocation density) and positron annihilation lifetime (PAL) parameters (i.e., defect-specific positron lifetime, the concentration of vacancy defect). We have thoroughly investigated various physical properties of pristine and Fe^{3+}-substituted $CaCu_3Ti_4O_{12}$ ceramics, $CaCu_{3-x}Ti_{4-x}Fe_{2x}O_{12}$ with x = 0.0–0.7, in recent years (2018–2021)[26–37]. In the system, divalent, weak magnetic (1 Bohr magneton), Jahn-Teller Cu^{2+} ions, and tetravalent, non-magnetic Ti^{4+} ions are simultaneously replaced by highly magnetic (5 Bohr magneton), trivalent Fe^{3+} ions in the series of quadruple perovskites, $CaCu_{3-x}Ti_{4-x}Fe_{2x}O_{12}$ where x varies from 0.0 to 0.7. Thus, interesting improvements in electrical behavior are expected. This work blends fundamental and applied research.

2. Experimental details

A series of cubic perovskites, $CaCu_{3-x}Ti_{4-x}Fe_{2x}O_{12}$ with x = 0.0, 0.1, 0.3, 0.5 and 0.7, was prepared by the mixed oxide route. The complete details regarding the synthesis, crystallographic phase identification, and structural parameters including cationic distribution determination by employing Rietveld refinement of X-ray powder diffraction data and average grain size (D) estimation by analyzing scanning electron micrographs are given elsewhere[27, 33]. The measurements of current (I) versus applied signal voltage (V) (V = 0–400 V) (*I*–*V* characteristics) were carried out with the help of an Aplab made high-voltage dc regulated power supply (model no.: 7332) at temperatures ranging from T = 300–673 K using the two probe pressure contact method and a horizontal electric furnace. The cylindrically pelletized samples were rubbed with fine glass paper to give mirror-polished surfaces, and then cleaned with dilute hydrochloric acid and dimethyl ketone. To have perfect ohmic contact, microcracks on the surfaces were filled with a rubbing of graphite, and finally Al-foil was also kept on the surface. Instead of *I*–*V* characteristics, the traces of J versus E are taken into consideration, which eases the comparison between the *I*–*V* characteristics of the samples with varying thickness and surface area. A bi-terminal pressure contact method was employed to carry out the dc electrical resistivity measurement. The same set of the ceramic pellets, sample holder, vertical electric furnace, temperature indicator with thermocouple, and temperature controller used for thermal variation of I versus V characteristics was used to carry out temperature-dependent dc resistivity measurement. The resistance was directly measured using a mega-ohm meter supplied by BPL India. The thermal variation of resistance was obtained by keeping a sample holder containing a cylindrically pelletized sample in a horizontal electric furnace. For *I*–*V* characteristics and dc resistivity measurements as a function of temperature, an indigenously designed and fabricated sample holder was used. The holder consists of two ceramic beads with supporting metal roads. The spring-loaded brass electrode is introduced into the ceramic beads and pressed hard against the surface of the pellet. The second brass electrode is fixed at the other end. GELCO electronics private limited, India made PTS-7201 temperature indicator attached with K-type chromal-alumel thermocouple were used to measure the temperature of the pellet. The temperature of the furnace was controlled by maintaining the current passing through the heater employing a current controller (Bharat electrical Mumbai, India, made single phase auto-transformer). The resistance was noted during the cooling cycle at an interval of 20 °C in the temperature range of 300–773 K. A single set of temperature-dependent *I*–*V* characteristics and dc resistivity measurements have been performed.

3. Results and discussion

A careful structural analysis demonstrates that the x = 0.0–0.5 compositions are formed in the single phase with cubic perovskite crystal symmetry in the space group Im3. For the composition with x = 0.7, the aciculate but low intensity

Table 1. Structural, microstructural, and electric parameters for a series of cubic perovskites.

Fe^{3+}– content (x)	Strain 10^{-4}	a (Å) ±0.002 Å	d_x (g/cm^3)	d (g/cm^3)	f	D (μm)	δ (10^{10} m^{-2})	T_{sL} (K)	E_s (V/cm) T = 473 K	J_{max} (mA/cm^2)	E_{a1} (eV)	E_{a2} (eV)
0.0	–4.54	7.391	5.056	4.744	0.062	3.7	7.30	473	978	327	0.33	0.43
0.1	–6.16	7.388	5.061	4.712	0.069	–	–	373	570	270	0.29	0.29
0.3	–6.77	7.387	5.064	4.704	0.071	7.5	1.78	373	525	225	0.22	0.21
0.5	–5.96	7.400	5.038	4.556	0.096	7.9	1.60	373	261	225	0.25	0.15
0.7	–6.95	7.411	5.016	4.566	0.090	3.4	8.65	373	300	225	0.27	0.21

T_{sL} is the lowest temperature at which switching action takes place. E_s is the threshold value of the electric field beyond which non-ohmic behavior is observed. J_{max} is the maximum current density value. E_{a1} and E_{a2} are the activation energies determined from Arrhenius plots below and above the transition temperature, respectively.

Table 2. Distribution of metallic cations (Ca^{+2}, Cu^{+2}, Ti^{+4} and Fe^{+3}) among the available crystallographic sites determined from Rietveld refinement of X-ray powder diffraction data (T = 300 K) for $CaCu_{3-x}Ti_4Fe_{2x}O_{12}$ (x = 0.0–0.7) system.

Fe^{3+} content (x)	Cation distribution
0.0	$Ca^{2+}[Cu_3^{2+}]\{Ti_4^{4+}\}O_{12}^{2-}$
0.1	$Ca^{2+}[Cu_{2.86}^{2+}Fe_{0.14}^{3+}]\{Ti_{3.90}^{4+}Fe_{0.06}^{3+}Cu_{0.04}^{2+}\}O_{12}^{2-}$
0.3	$Ca^{2+}[Cu_{2.41}^{2+}Ti_{0.24}^{4+}Fe_{0.35}^{3+}]\{Ti_{3.46}^{4+}Fe_{0.25}^{3+}Cu_{0.29}^{2+}\}O_{12}^{2-}$
0.5	$Ca^{2+}[Cu_{2.03}^{2+}Ti_{0.17}^{4+}Fe_{0.80}^{3+}]\{Ti_{3.33}^{4+}Fe_{0.20}^{3+}Cu_{0.47}^{2+}\}O_{12}^{2-}$
0.7	$Ca^{2+}[Cu_{1.53}^{2+}Ti_{0.12}^{4+}Fe_{1.35}^{3+}]\{Ti_{3.18}^{4+}Fe_{0.05}^{3+}Cu_{0.77}^{2+}\}O_{12}^{2-}$

(~ 4.0 %) peak centered at 2θ = 25.6° is due to a trivial amount of anatase structure of well-crystallized TiO_2[33]. The secondary phase is randomly distributed within the primary $CaCu_3Ti_4O_{12}$ matrix. Thus, Fe^{3+} substitution is restricted to x = 0.7 in the present study. In Tables 1 and 2, the structural and microstructural parameters are compiled to illustrate the compositional and temperature-dependent J–E characteristics.

Fig. 1 gives the plots of J against E registered at different temperatures ranging from T = 300–773 K for the series $CaCu_{3-x}Ti_{4-x}Fe_{2x}O_{12}$. The samples exhibit strong non-ohmic characteristics. In the low E region, the dominant conduction mechanism is thermal excitation and as a result the J–E curve is nearly ohmic. Nonlinear behavior is observed when E is beyond the particular threshold value or breakdown value (E_s) ($E > E_s$). In this regime, tunneling action via grain-boundary barrier is responsible for the electric conduction. It is seen in Fig. 1 that the lowest temperature at which switching action takes place (T_{sL}) decreases with Fe-content (x). The compositions with x = 0.0, (0.1, 0.3, 0.5) and 0.7 show switching action for $T \geqslant$ 473 K, ($T \geqslant$ 373 K), $T \geqslant$ 313 K, respectively. Meanwhile, E_s decreases with x for x = 0.0 to 0.5 compositions, while for x = 0.7 composition E_s shows small enhancement (Table 1). The compositional variation of E_s may be described by considering the structural and microstructural parameters. The strain values have been deduced from the simple and widely employed Williamson-Hall plot method[38]. The negative slope for all of the compositions suggests that a compressive strain has been produced (Fig. 2). The strain increases from -4.54×10^{-4} for x = 0.0 composition to -6.77×10^{-4} for x = 0.3 composition, it then decreases to -5.96×10^{-4} for x = 0.5 composition and further increases to -6.95×10^{-4} for x = 0.7 composition. It has been reported elsewhere that strain is directly proportional to T_{sL} and E_s, values[26] but no such correlation has been observed in this work. Hu *et al.*[39] have shown that for ceramically prepared compositions, E_s is inversely proportional to aggregate grain size (D) ($E_s \propto 1/D$). For the series under investigation, D increases from 3.7 μm for x = 0.0 composition to 7.9 μm for x = 0.5 composition and then abruptly decreases to 3.4 μm for x = 0.7 composition[33]. The increase of D means that there is a decrease in the number of grain-boundary barriers. Accordingly, E_s decreases from 978 V/cm for x = 0.0 composition to 261 V/cm for x = 0.5 composition and then for x = 0.7 composition E_s slightly increases to 300 V/cm, as shown in Table 1. Furthermore, observed decrease in T_{sL} and E_s for x = 0.0 – 0.3 compositions may be correlated with a subsequent decrease in lattice parameter (a (Å))[38] (Table 1). The observed decrease in a with Fe-substitution (x) for the composition x = 0.0–0.3 infers that charge carriers need a small amount of energy for the conduction and thus T_{sL} and E_s decrease for x = 0.0–0.3 compositions. The observed dependence of E_s with Fe- content (x) can also be explained based on defects that occur during the sintering process. There are three types of defects: vacancy, dislocation, and grain boundary. The presence of these defects effectively modifies the material's optical and electrical properties. It has been reported that interface defect density or dislocation density on grain boundaries (δ) $\propto 1/D^2 \propto E_s^2$ [26,38]. Thus, on increasing grain size from x = 0.0–0.5 compositions and observed grain size reduction for x = 0.7 composition turned into decrease in δ and E_s values (x = 0.0–0.5) and increase in δ and E_s values for x = 0.7 composition as observed (Table 1). The concentration of vacancy defects (C_d) determined from highly sophisticated PAL spectroscopy measurements[29] decreases rapidly within the crystallites for x = 0.0–0.3 compositions and then saturates gradually for x = 0.5 and 0.7 compositions. The variation of C_d is consistent with the variation of E_s with Fe^{3+}-content (x). This leads to a very important conclusion that the E_s is mainly controlled by C_d and δ.

Another interesting observation from Fig. 1 is that maximum current density (J_{max}) decreases from 327 mA/cm^2 for x = 0.0 composition to 270 mA/cm^2 for x = 0.1 composition to 225 mA/cm^2 for x = 0.3 composition and remains constant with further Fe^{3+}-substitution. In the design of electronic and electrical devices, current density has a very significant role. Over the last few years, there has been a movement towards having a higher current density to achieve a higher number of devices in an ever-smaller chip area. As discussed earlier, with an increase in D for x = 0.0–0.5 compositions, the contribution from poorly conducting grain boundaries decreases as compared to semiconducting grains; thus, J_{max} is expected to increase with Fe- substitution, but this is not the case. This suggests that besides grain size, other microstructural parameters are also expected to affect J_{max}. Zheng *et al.*[40], following the density functional theory, have shown that in $CaCu_3Ti_4O_{12}$ the conduction mechanism is an adiabatic hop-

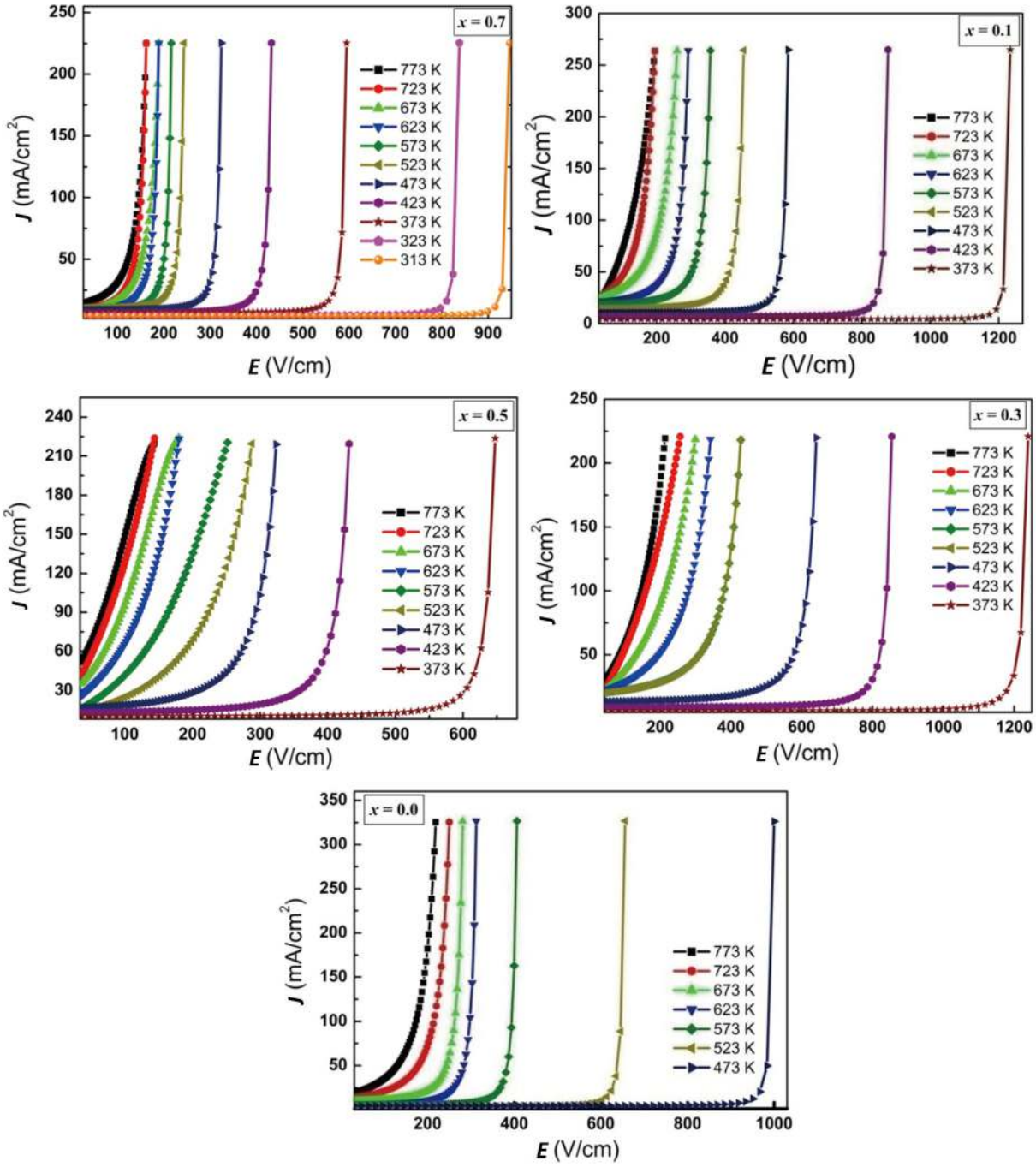

Fig. 1. (Color online) Plots of *J*–*E* characteristic recorded at different temperatures for a series of cubic perovskites, $CaCu_{3-x}Ti_{4-x}Fe_{2x}O_{12}$ (x = 0.0–0.7).

ping conduction of small polarons and electron transport among CuO_4 square-planar (A´-site) clusters. Furthermore, the conduction band is chiefly contributed by the antibonding states of Cu 3*d* electrons. Usually, metal oxide series containing Jahn-Teller ions (high-spin d^4 Cr^{2+} and Mn^{3+} ions, low-spin d^7 Co^{2+} and d^9 Cu^{2+} ions) are referred to as the most likely candidates to demonstrate switching action. Based on the above findings, it is clear that cupric ions on the A´-site play a governing role in switching phenomenon and electric conduction. It is now feasible to elucidate the compositional variation of J_{max}. The occupancy of metallic cations such as Ca^{2+}, Cu^{2+}, Ti^{4+} and Fe^{3+} among the crystallographic interstitial sites determined from Rietveld refinement of X-ray diffraction patterns revealed that with Fe- substitution the Cu^{2+}-ion concentration at the A´ decreases from 3.0 for x = 0.0 composition to 1.53 for x = 0.7 composition[29, 33], as displayed in Table 2. This results in the curtailment of electric conduction through the square-planar site, and thus J_{max} decreases rapidly for x = 0.0–0.3 compositions and then levels off for the compositions with x = 0.5 and 0.7, as shown in Table 1. The observed reduction in J_{max} for x = 0.7 composition can also be explained based on the formation of a minor secondary insulating TiO_2-phase and reduced grain size. The percentage formation of these secondary phases is well below the theoretical percolation threshold (~16%) and experimental percolation threshold (~20%) values. This would ensure that electric behavior such as E_s and J_{max} would always be dominated by the $CaCu_3Ti_4O_{12}$ phase[33]. An effort has been undertaken to correl-

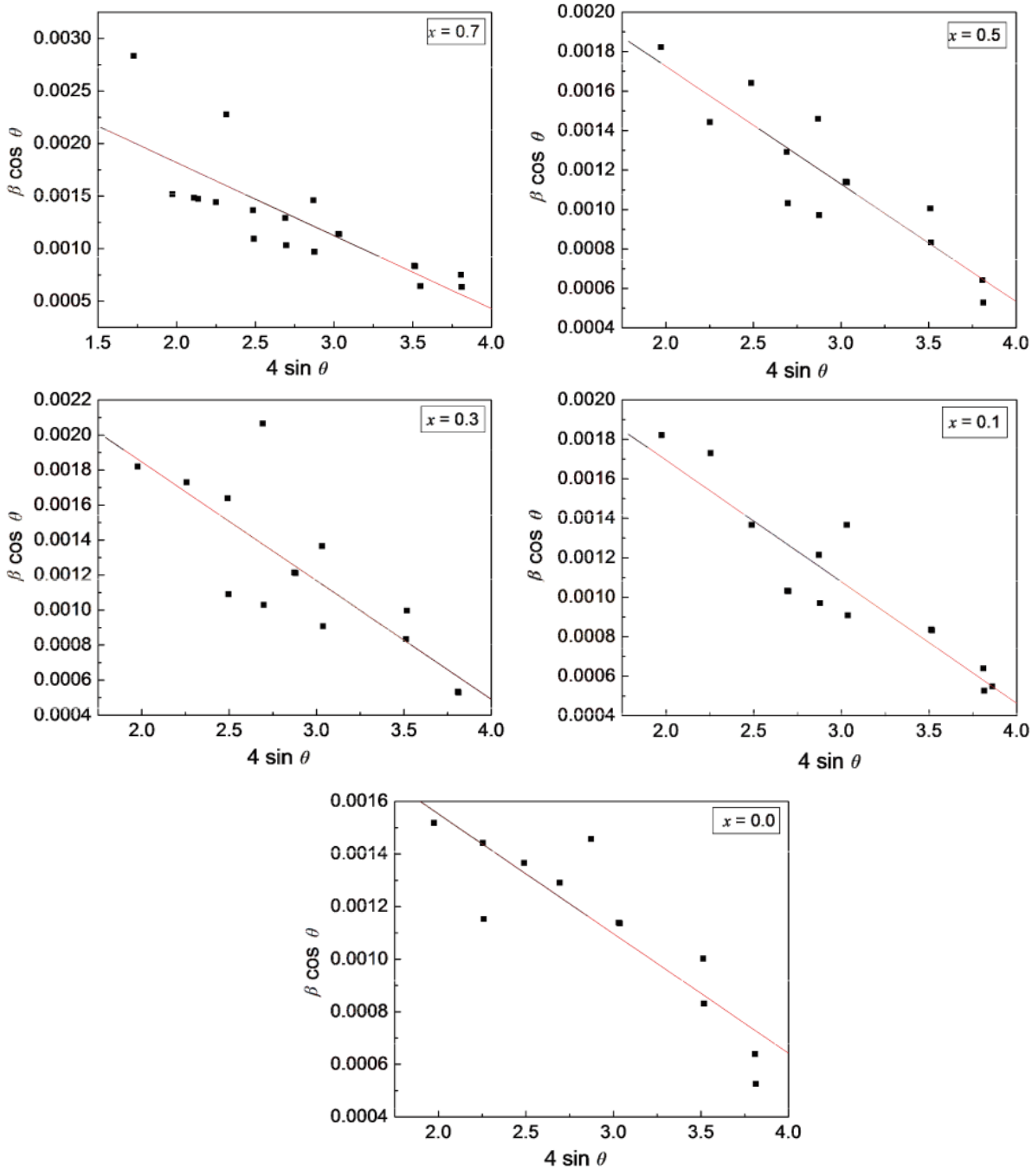

Fig. 2. Williamson-Hall plots for all the samples of a series $CaCu_{3-x}Ti_{4-x}Fe_{2x}O_{12}$.

ate the previous outcome of the PAL spectroscopy study[29] and present electric parameters as a function of composition (x). The magnitude of defect-specific positron lifetime (τ_2) reflects the contributions from the grain boundaries, vacancies, and vacancy clusters in grains. Earlier, it was found that τ_2 gradually increases from 0.2317 ns for x = 0.0 composition to 0.4449 ns for x = 0.5 composition and then level off for x = 0.7 composition to 0.4379 ns. The subsequent increase in τ_2 suggests that the thickness of grain-boundary layers increases with Fe-substitution for x = 0.0–0.5 compositions and saturate for x = 0.7 compositions. This limits the conduction of charge carriers from one conducting grain to the adjacent conducting grain separated by the highly resistive grain boundary. This is thought to be the cause of the observed initial reduction of J_{max} with x. On the same line of argument, E_s is expected to increase with x but no such trend has been observed. This suggests that as far as E_s value is concerned, an increase in grain size and decrease in defect density in grains dominant over the grain boundary broadening with Fe^{3+}- substitution in the system, $CaCu_{3-x}Ti_{4-x}Fe_{2x}O_{12}$.

To the best of our knowledge, these values of J_{max} for the pure and Fe-substituted $CaCu_3Ti_4O_{12}$ ceramics are the highest ever reported values, except for those reported for Nb^{5+} and Ta^{5+}-substituted $CaCu_3Ti_4O_{12}$ ($J_{max} \approx 275$ mA/cm^2)[41]. Earlier, we have found J_{max} = 254 mA/cm^2 and 234 mA/cm^2 for quenched and microwave-assisted samples of $CaCu_3Ti_4O_{12}$, respectively[26]. The nanocrystalline and microcrystalline samples of $CaCu_3Ti_4O_{12}$ synthesized by distinct routes (solid-state reaction, sol-gel, modified sol-gel, thermal decomposition, spark plasma sintering etc.) and treated with different conditions (at-

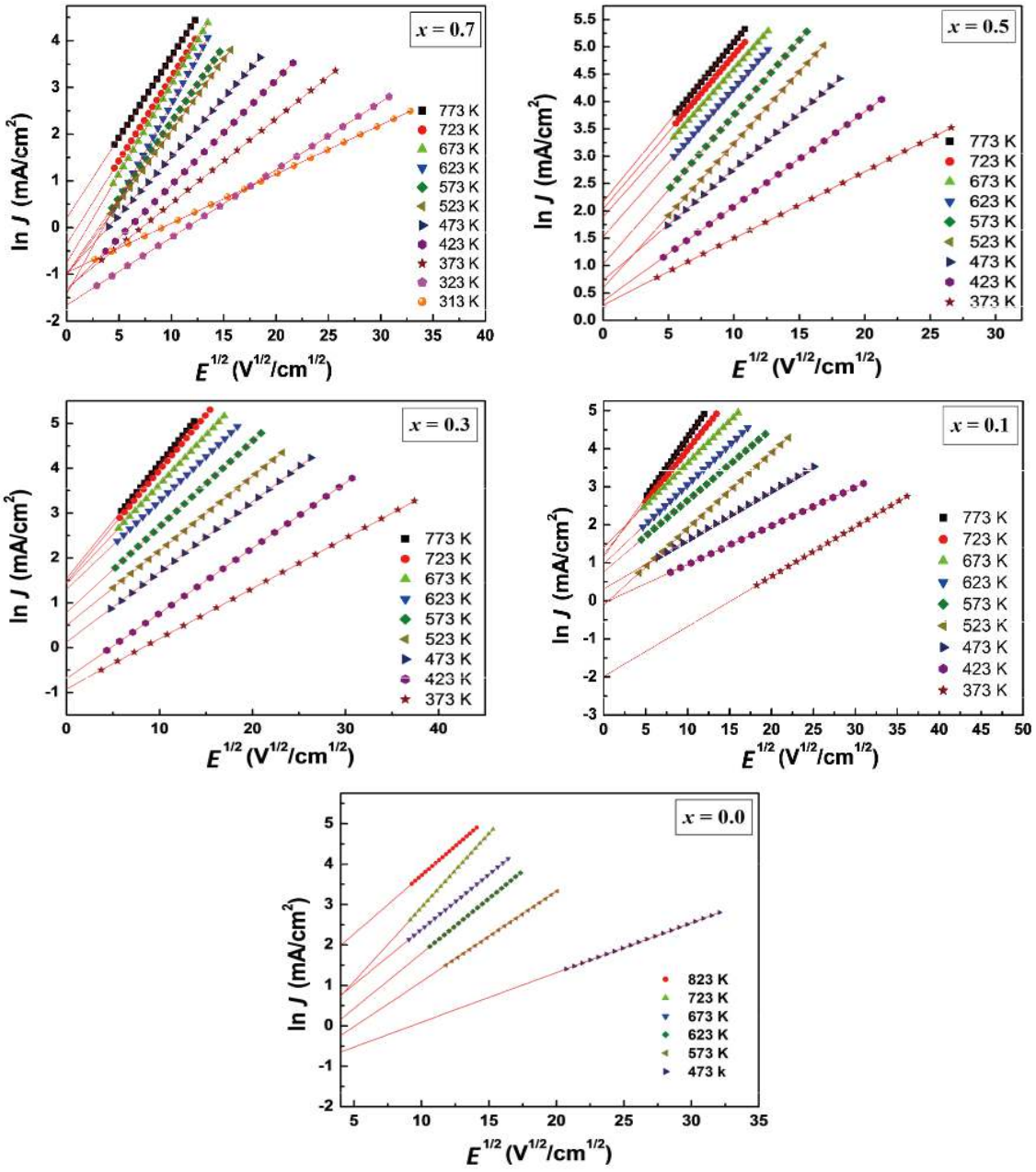

Fig. 3. (Color online) ln J against $E^{1/2}$ plots at different temperatures for polycrystalline samples of quadruple perovskite series, $CaCu_{3-x}Ti_{4-x}Fe_{2x}O_{12}$.

moshphere, sintering temperature and duration etc.) have shown that J_{max} varies from 0.1–32 mA/cm^2[3, 42–48]. Meanwhile, Y and Mg co-doped samples of $CaCu_3Ti_4O_{12}$ have shown $J_{max} \approx 28$ mA/cm^2[49], Sr-Ni substituted $CaCu_3Ti_4O_{12}$ have exhibited $J_{max} \approx 15$ mA/cm^2[14], Pr-substituted $CaCu_3Ti_4O_{12}$ have demonstrated $J_{max} = 15$ mA/cm^2[50], while Zn + Zr co-doped $CaCu_3Ti_4O_{12}$ thin films show J_{max} in the range of 5–6 mA/cm^2[51]. Finally, the composites, $(1-x)(CaCu_3Ti_4O_{12})-(x)(0.1\ Na_{0.5}\ Bi_{0.5}TiO_3-0.9\ BaTiO_3)$ with $x = 0.02$, 0.04, 0.06, 0.08 and 0.10, have shown J_{max} ranging from 13–20 mA/cm^2[52].

The existence of the Schottky barrier at the grain boundaries is signified by the observed linear relationship for ln J against $E^{1/2}$ traces[53–55] (Fig. 3). The Schottky barrier height (ϕ_B) values determined from the slopes of the fitting lines of ln J_0 (J_0 is the value of J extrapolated to $E = 0$ V/cm) against reciprocal of temperature 1000/T graphs (Fig. 4) decreases from 0.25 eV for $x = 0.0$ composition to 0.21 eV for $x = 0.5$ composition while ϕ_B value increases to 0.28 eV for $x = 0.7$ compositions. The electric potential barrier height for the pristine composition, $CaCu_3Ti_4O_{12}$ is consistent with the reported value[56]. Huang *et al.*[54] have shown that the ϕ_B is influenced by the residual impurities and impurities from decomposition. The ϕ_B demonstrates a close linear relationship to the microstrain and δ.

The coefficient of determination (R^2) of a statistical model describes how well it fits a set of observations. A measure of this goodness-of-fit typically summarizes the discrepancy between the observed values and the values expected under the model in question. The R^2 value between 0.70–1.0 indicates that there is a strong correlation between the dependent and independent variables. In general, R^2 value at or above 0.60 is considered to be worthwhile[57].

On fitting ln J_0 versus reciprocal of temperature (1000/T)

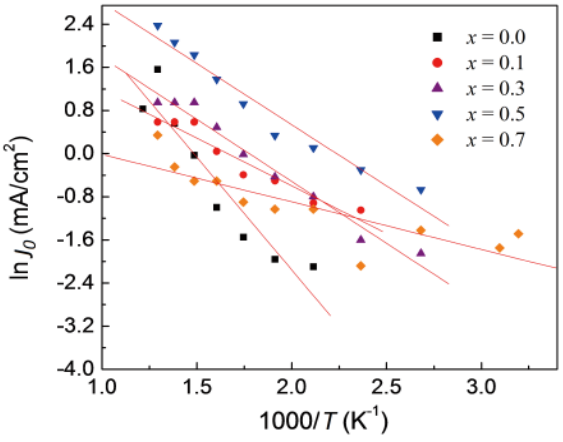

Fig. 4. (Color online) Plots of ln J_o against temperature for the different compositions.

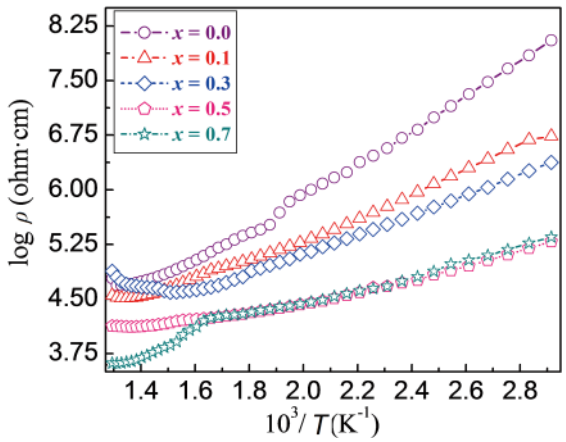

Fig. 5. (Color online) Arrhenius plots for a quadruple perovskite series, $CaCu_{3-x}Ti_{4-x}Fe_{2x}O_{12}$.

plots with linear relation, the R^2 value for x = 0.0 composition is found to be 0.91, for x = 0.1 composition, R^2 = 0.94, for x = 0.3 composition, R^2 = 0.97, for x = 0.5 composition, R^2 = 0.95 and for the composition with x = 0.7, R^2 comes to 0.90. These values of R^2 are near the ideal value of 1.0, which suggests that the applied carrier transport model is able to successfully and accurately model the experimental data.

When we think about the varistor-type device, two parameters (i.e., non-linearity coefficient (α) and E_s) are considered as a figure-of-merit. A large value of α is always desirable because it allows the device to withstand the surges at E_s. The α values at different temperatures were calculated for the compositions with x = 0.0–0.7 using the standard definition. The α value is found to vary from 2.09–4.51, 0.45–1.14, 0.60–1.64, 0.76–2.34, and 1.27–6.88 for x = 0.0, 0.1, 0.3, 0.5 and 0.7 compositions, respectively, in the studied range of temperature. Furthermore, the value of α is found to increase with temperature and Fe-substitution (x) (x = 0.1–0.7). This can be explained as follows.

The nonlinear coefficient (α) is defined by the standard relation: $\alpha = (\log J_2 - \log J_1) / (\log E_2 - \log E_1)$, where J_1 and J_2 are calculated analogous to I_1 = 1 mA and I_2 = 10 mA, respectively, and E_1 and E_2 are the corresponding values of the electric fields. The electric field (E) and threshold voltage (E_s) decrease with increasing Fe^{3+}-substitution (x) in the system, $CaCu_{3-x}Ti_{4-x}Fe_{2x}O_{12}$, for x = 0.0–0.5 compositions. This is attributed to the decrease of the number of grain boundaries due to the increase of average grain size[58] from 3.7 μm for x = 0.0 composition to 7.9 μm for x = 0.5 composition, as depicted in Table 1. Meanwhile, with an increase in temperature and the concentration of highly magnetic Fe^{3+}-ions (5μ_B) for non-magnetic Ti^{4+} (0 μ_B) in the system, the degree of $Fe^{3+} + e^- \rightarrow Fe^{2+}$ conduction that occurs on the square-planar site of the cubic perovskite structure is enhanced. Thus, I and J are expected to increase. These combined effects result in an increase in the value of α with temperature and Fe^{3+}-substitution (x). The ranges of α value advise that these perovskites are best suited for low-voltage varistor applications. In the literature, a wide range of α values ranging from α = 1.91 to α = 912 have been reported for pristine composition, $CaCu_3Ti_4O_{12}$, registered at different temperatures, and synthesized with different sintering temperatures, preparative parameters, preparation routes, thermal history, voltage rise time in bulk, nanocrystalline and thin-film forms[26].

The high-temperature synthesis process of oxide ceramics that is employed here leads to the inevitable formation and existence of pores. Thus, X-ray density (d_x) is always higher than the bulk density (d). These voids decisively affect the electric, dielectric, and elastic properties of the material. Thus, it is essential to correct such parameters for a void-free state, especially for compositional dependent investigation. The dc resistivity values in the void-free state (ρ_{dc}) for the different compositions have been determined from the experimental values of dc resistivity (ρ_p) recorded at different temperatures and void fraction values ($f = 1 - (d/d_x)$) with the help of the following relation [59] :

$$\rho_{dc} = \rho_p \left[1 + f(1 + f^{2/3})^{-1}\right]^{-1},$$

This relation is effectively applied for the materials having $f < 0.4$. The different compositions of the system under study possess f values that are much less than 0.4, as shown in Table 1. The ρ_{dc} values for x = 0.0–0.7 compositions lie in the range10^5–10^8 Ω·cm at T = 300 K, advising that these are good insulating materials. Fig. 5 portrays log ρ versus temperature plots (Arrhenius plot). All of the compositions reveal usual semiconducting behavior (i.e., a decrease of resistivity with temperature). In the low-temperature regime, 300 K ⩽ T ⩽ 573 K, a linear variation of resistivity with temperature is observed; while for T > 573 K, a discontinuity or change of slope occurs, suggesting a change in the mechanism responsible for conduction in the studied materials. This may be correlated with the diffuse anomaly that takes place at T = 630 K[60] or may be associated with high-temperature structural phase transition reported occurring between T = 726–732 K for pure $CaCu_3Ti_4O_{12}$ composition[61]. The activation energy values (E_{a1} and E_{a2}) were calculated for regions below and above the transition temperature, respectively, from the well-known Arrhenius equation and are shown in Table 1. In the low-temperature region, T = 300–573 K, E_{a1} decreases from 0.33 eV for x = 0.0 composition to 0.22 eV for x = 0.3 composition, and then increases to 0.25 and 0.27 eV for x = 0.5 and 0.7 compositions, respectively. The lattice constant (a) value decreases from 7.391 Å for x = 0.0 composition to 7.387 Å for x = 0.3 composition, and then increases to 7.400 and 7.411 Å for x = 0.5 and 0.7 compositions, respectively (Table 1). The observed reduction in a with x suggests a corresponding de-

crease in interionic distances and as a result a decrease in barrier height encountered by the hopping charge carriers. Thus, E_{a1} is supposed to decrease for x = 0.0–0.3 compositions. The same argument is applicable for the observed increase in E_{a1} with an increase in a for x = 0.5 and 0.7 compositions. The average size of grains (D) also affects E_{a1}[62]. A bigger grain size insinuates increased grain-to-grain contact area for the charge carrier to flow and consequently a lower barrier height, and vice versa. As discussed above, D increases from 3.7 μm for x = 0.0 composition to 7.9 μm for x = 0.5 composition and then decrease to 3.4 μm for x = 0.7 composition. This explains the observed dependence of E_{a1} with Fe-content (x). The E_{a1} values ranging from 0.22–0.33 eV are much higher than the ionization energy of acceptors and donors (i.e., 0.1 eV), and thus band-type conduction may not be possible. These values lie between the activation energy of a small polaron ($\geqslant$ 0.5 eV) and the energy needed for the electron hopping mechanism (0.2 eV). Thus, the conduction proceeds by electrons with deformation. The E_{a2} for the high-temperature regime are 0.43, 0.29, 0.21, 0.15, 0.21 eV, respectively, for x = 0.0, 0.1, 0.3, 0.5 and 0.7 compositions. Commonly, the resistivity of oxide ceramics is essentially dependent on the mobility and concentration of the carrier, but at such relatively low temperature it cannot be ascribed to oxygen depletion or absorption. The observed high-temperature deviation may be the result of the vacancy-disorder transition. Oxygen vacancies become ordered in the low-temperature regime, considerably enhancing the resistivity and thus higher activation energy. In the high-temperature regime, the conduction process is contributed by the oxygen ions and the oxygen vacancies are disordered, which allows oxygen ions to migrate with lower activation energy[25]. Furthermore, in the temperature range studied, resistivity decreases with Fe^{3+}-concentration (x). The incorporation of highly magnetic Fe^{3+} ions which take part in the process of conduction, for non-magnetic Ti^{4+} ions, enhances the degree of $Fe^{3+} + e^{-} = Fe^{2+}$ conduction that occurs on the A´ - site of the cubic perovskite structure. Thus, dc resistivity decreases with Fe^{3+}-substitution.

4. Conclusions

The following conclusions can be drawn based on the electrical properties studies of a series of quadruple perovskites, $CaCu_{3-x}Ti_{4-x}Fe_{2x}O_{12}$ where x = 0.0–0.7. The switching action is chiefly due to the concentration of Jahn-Teller Cu^{2+} ion engendered distortion in the system. The variation of switching temperature and threshold field is principally governed by grain size, interface defect density, and vacancy defects but not by compressive strain. The J_{max} value is controlled by a change in Cu^{2+} ion concentration on the A´-site and the thickness of the grain-boundary layer on Fe^{3+}-substitution. It is possible to tailor electrical parameters by controlling the structural and microstructural parameters, which is important from an application's point of view. The system is found to be suitable for low-voltage varistor applications. The compositional dependence of dc resistivity is governed by ferric ion concentration on the square-planar site of cubic perovskite structure and the activation energy values are suggestive of conduction through electrons with deformation.

Acknowledgements

One of the authors (DJP) is thankful to the Education Department, Gujarat state for providing financial assistance under ScHeme of developing high-quality research (SHODH).

References

[1] Subramanian M A, Li D, Duan N, et al. High dielectric constant in $ACu_3Ti_4O_{12}$ and $ACu_3Ti_3FeO_{12}$ phases. J Solid State Chem, 2000, 151, 323

[2] Ramirez A P, Subramanian M A, Gardel M, et al. Giant dielectric constant response in a copper-titanate. Solid State Commun, 2000, 115, 217

[3] Prompa K, Swatsitang E, Saiyasombat C, et al. Very high performance dielectric and non-Ohmics properties of $CaCu_3Ti_{4.2}O_{12}$ ceramics for X8R capacitors. Ceram Int, 2018, 44, 13267

[4] Kretly L C, Almeida A F L, de Oliveira R S, et al. Electrical and optical properties of $CaCu_3Ti_4O_{12}$ (CCTO) substrates for microwave devices and antennas. Microw Opt Technol Lett, 2003, 39, 145

[5] Chung S Y, Kim I D, Kang S J L. Strong nonlinear current-voltage behaviour in perovskite-derivative calcium copper titanate. Nat Mater, 2004, 3, 774

[6] Felix A A, Rupp J L M, Varela J A, et al. Multi-functional properties of $CaCu_3Ti_4O_{12}$ thin films. J Appl Phys, 2012, 112, 054512

[7] Kushwaha H S, Madhar N A, Ilahi B, et al. Efficient solar energy conversion using $CaCu_3Ti_4O_{12}$ photoanode for photocatalysis and photoelectrocatalysis. Sci Rep, 2016, 6, 1

[8] Chhetry A, Sharma S, Yoon H, et al. Enhanced sensitivity of capacitive pressure and strain sensor based on $CaCu_3Ti_4O_{12}$ wrapped hybrid sponge for wearable applications. Adv Funct Mater, 2020, 30, 1910020

[9] Chattopadhyay A, Nayak J. Synthesis of CCTO powder for application in humidity sensor. AIP Conference Proceedings, 2020, 040020

[10] Prompa K, Swatsitang E, Putjuso T. Enhancement of nonlinear electrical properties with high performance dielectric properties of $CaCu_{2.95}Cr_{0.05}Ti_{4.1}O_{12}$ ceramics. Ceram Int, 2018, 44, S72

[11] Ren L L, Yang L J, Xu C, et al. Improvement of breakdown field and dielectric properties of $CaCu_3Ti_4O_{12}$ ceramics by Bi and Al co-doping. J Alloys Compd, 2018, 768, 652

[12] Boonlakhorn J, Thongbai P. Dielectric properties, nonlinear electrical response and microstructural evolution of $CaCu_3Ti_{4-x}Sn_xO_{12}$ ceramics prepared by a double ball-milling process. Ceram Int, 2020, 46, 4952

[13] Cortés J A, Cotrim G, Orrego S, et al. Dielectric and non-ohmic properties of $Ca_2Cu_2Ti_{4-x}Sn_xO_{12}$ ($0.0 \leqslant x \leqslant 4.0$) multiphasic ceramic composites. J Alloys Compd, 2018, 735, 140

[14] Rhouma S, Saîd S, Autret C, et al. Comparative studies of pure, Sr-doped, Ni-doped and co-doped $CaCu_3Ti_4O_{12}$ ceramics: Enhancement of dielectric properties. J Alloys Compd, 2017, 717, 121

[15] Wu S, Liu P, Lai Y M, et al. Effect of Ba^{2+} doping on microstructure and electric properties of calcium copper titanate ($CaCu_3Ti_4O_{12}$) ceramics. J Mater Sci: Mater Electron, 2016, 27, 10336

[16] Barman N, Varma K B R. Enhanced non-linear current-voltage response of Te-doped calcium copper titanate ceramics. Ceram Int, 2017, 43, 6363

[17] Grzebielucka E C, Leandro Monteiro J F H, de Souza E C F, et al. Improvement in varistor properties of $CaCu_3Ti_4O_{12}$ ceramics by chromium addition. J Mater Sci Technol, 2020, 41, 12

[18] Sun J J, Xu C, Zhao X T, et al. Improved dielectric properties of indium and tantalum co-doped $CaCu_3Ti_4O_{12}$ ceramic prepared by spark plasma sintering. IEEE Trans Dielectr Electr Insul, 2020, 27, 1400

[19] Sripakdee C, Prompa K, Swatsitang E, et al. Very high-performance dielectric and non-ohmic properties of novel X8R type $Ca_{1-1.5x}Ho_xCu_3Ti_4O_{12}/TiO_2$ ceramics. J Alloys Compd, 2019, 779,

521
[20] Boonlakhorn J, Chanlek N, Manyam J, et al. Enhanced giant dielectric properties and improved nonlinear electrical response in acceptor-donor (Al^{3+}, Ta^{5+})-substituted $CaCu_3Ti_4O_{12}$ ceramics. J Adv Ceram, 2021, 10, 1243
[21] Löhnert R, Bartsch H, Schmidt R, et al. Microstructure and electric properties of $CaCu_3Ti_4O_{12}$ multilayer capacitors. J Am Ceram Soc, 2015, 98, 141
[22] Zheng Q, Fan H Q, Long C B. Microstructures and electrical responses of pure and chromium-doped $CaCu_3Ti_4O_{12}$ ceramics. J Alloys Compd, 2012, 511, 90
[23] Amhil S, Choukri E, Ben Moumen S, et al. Evidence of large hopping polaron conduction process in strontium doped calcium copper titanate ceramics. Phys B, 2019, 556, 36
[24] Fan H Q, Zheng Q, Peng B L. Microstructure, dielectric and pyroelectric properties of $CaCu_3Ti_4O_{12}$ ceramics fabricated by tape-casting method. Mater Res Bull, 2013, 48, 3278
[25] Chen L, Chen C L, Lin Y, et al. High temperature electrical properties of highly epitaxial $CaCu_3Ti_4O_{12}$ thin films on (001) $LaAlO_3$. Appl Phys Lett, 2003, 82, 2317
[26] Raval P Y, Makadiya A R, Pansara P R, et al. Effect of thermal history on structural, microstructural properties and *J*– *E* characteristics of $CaCu_3Ti_4O_{12}$ polycrystalline ceramic. Mater Chem Phys, 2018, 212, 343
[27] Pansara P R, Raval P Y, Vasoya N H, et al. Intriguing structural and magnetic properties correlation study on Fe^{3+}-substituted calcium-copper-titanate. Phys Chem Chem Phys, 2018, 20, 1914
[28] Raval P Y, Pansara P R, Vasoya N H, et al. Positron annihilation spectroscopic investigation of high energy ball - milling engendered defects in $CaCu_3Ti_4O_{12}$. Ceram Int, 2018, 44, 15887
[29] Pansara P R, Meshiya U M, Makadiya A R, et al. Defect structure transformation during substitution in quadruple perovskite $CaCu_{3-x}Ti_{4-x}Fe_{2x}O_{12}$ studied by positron annihilation spectroscopy. Ceram Int, 2019, 45, 18599
[30] Raval P Y, Pansara P R, Makadiya A R, et al. Investigation on external stimuli engendered magnetic ordering in polycrystalline $CaCu_3Ti_4O_{12}$ quadruple perovskite. Ceram Int, 2018, 44, 17667
[31] Meshiya U M, Raval P Y, Pansara P R, et al. Electronic structure, orbital symmetry transformation, charge transfer, and valence state studies on Fe^{3+}-substituted $CaCu_3Ti_4O_{12}$ quadruple perovskites using X-ray photoelectron spectroscopy. Ceram Int, 2020, 46, 2147
[32] Raval P Y, Pansara P R, Vasoya N H, et al. First observation of reversible mechanochromism and chromaticity study on calcium-copper-titanate. J Am Ceram Soc, 2019, 102, 6872
[33] Raval P Y, Joshi N P, Pansara P R, et al. A Ti $L_{3,2}$- and *K*- edge XANES and EXAFS study on Fe^{3+}-substituted $CaCu_3Ti_4O_{12}$. Ceram Int, 2018, 44, 20716
[34] Meshiya U M, Jani K K, Mange P L, et al. Defect characterization of slow-cooled and quenched samples of calcium-copper-titanate through positron annihilation spectroscopy. Spectrosc Lett, 2019, 52, 633
[35] Pansara P R, Raval P Y, Pandit R, et al. First experimental evidence of non-collinear spin structure in $CaCu_{2.3}Ti_{3.3}Fe_{1.4}O_{12}$. Ceram Int, 2020, 46, 10016
[36] Meshiya U M, Raval P Y, Joshi N P, et al. Probing Fano resonance, relaxor ferroelectricity, light scattering by orbital exchange-bond, orbitons by Raman spectroscopy, and their correlation with dielectric properties of pure and Fe^{3+} - substituted calcium-copper-titanate. Vib Spectrosc, 2021, 112, 103201
[37] Raval P Y, Pansara P R, Chen C L, et al. Probing reversal of orbital symmetry in $CaCu_{3-x}Ti_{4-x}Fe_{2x}O_{12}$ (x = 0.0–0.7) by X-ray absorption spectroscopy. J Mater Sci: Mater Electron, 2021, 32, 13630
[38] Modi K B, Vasoya N H, Pathak T K, et al. Observation of CCNR-type electrical switching in $Zn_{0.3}Mn_{0.7+x}Si_xFe_{2-2x}O_4$ spinel ferrite series. SN Appl Sci, 2020, 2, 1840
[39] Hu W, Qin N, Wu G H, et al. Opportunity of spinel ferrite materials in nonvolatile memory device applications based on their resistive switching performances. J Am Chem Soc, 2012, 134, 14658
[40] Zheng P, Zhang R Z, Chen H Y, et al. Thermoelectric properties and conduction mechanism of $CaCu_3Ti_4O_{12}$ ceramics at high temperatures. J Electron Mater, 2014, 43, 1645
[41] Chung S Y, Choi J H, Choi J K. Tunable current-voltage characteristics in polycrystalline calcium copper titanate. Appl Phys Lett, 2007, 91, 091912
[42] Mao P, Wang J P, Liu S J, et al. Grain size effect on the dielectric and non-ohmic properties of $CaCu_3Ti_4O_{12}$ ceramics prepared by the Sol-gel process. J Alloys Compd, 2019, 778, 625
[43] Zhao X T, Ren L L, Yang L J, et al. Structure and dielectric relaxations of $CaCu_3Ti_4O_{12}$ ceramics by heat treatments in different atmospheres. IEEE Trans Dielectr Electr Insul, 2017, 24, 764
[44] Li T, He H F, Zhang T, et al. Effect of synthesizing temperatures on the microstructure and electrical property of $CaCu_3Ti_4O_{12}$ ceramics prepared by sol-gel process. J Alloys Compd, 2016, 684, 315
[45] Putjuso S, Nunglek S, Putjuso T. Nonlinear current-voltage and dielectric properties of $CaCu_3Ti_4O_{12}$ ceramics prepared by an aloe vera solution method. RMUTSB Acad J, 2016, 4, 172
[46] Kaur S, Kumar A, Sharma A L, et al. Dielectric and energy storage behavior of $CaCu_3Ti_4O_{12}$ nanoparticles for capacitor application. Ceram Int, 2019, 45, 7743
[47] Tang Z, Wu K N, Huang Y W, et al. High breakdown field $CaCu_3Ti_4O_{12}$ ceramics: Roles of the secondary phase and of Sr doping. Energies, 2017, 10, 1031
[48] Lin H, He X, Gong Y Y, et al. Tuning the nonlinear current-voltage behavior of $CaCu_3Ti_4O_{12}$ ceramics by spark plasma sintering. Ceram Int, 2018, 44, 8650
[49] Boonlakhorn J, Putasaeng B, Kidkhunthod P, et al. Improved dielectric properties of (Y + Mg) co-doped $CaCu_3Ti_4O_{12}$ ceramics by controlling geometric and intrinsic properties of grain boundaries. Mater Des, 2016, 92, 494
[50] Swatsitang E, Putjuso T. Very low loss tangent, high dielectric and non-ohmic properties of $Ca_{1-1.5x}Pr_xCu_3Ti_4O_{12}$ ceramics prepared by the sol-gel process. J Mater Sci: Mater Electron, 2017, 28, 18966
[51] Xu D, Yue X N, Song J, et al. Improved dielectric and non-ohmic properties of (Zn + Zr) codoped $CaCu_3Ti_4O_{12}$ thin films. Ceram Int, 2019, 45, 11421
[52] Mao P, Wang J P, Zhang L X, et al. Significantly enhanced breakdown field with high grain boundary resistance and dielectric response in $0.1Na_{0.5}Bi_{0.5}TiO_3$-$0.9BaTiO_3$ doped $CaCu_3Ti_4O_{12}$ ceramics. J Eur Ceram Soc, 2020, 40, 3011
[53] Zang G Z, Zhang J L, Zheng P, et al. Grain boundary effect on the dielectric properties of $CaCu_3Ti_4O_{12}$ ceramics. J Phys D, 2005, 38, 1824
[54] Huang Y M, Shi D P, Li Y H, et al. Effect of holding time on the dielectric properties and non-ohmic behavior of $CaCu_3Ti_4O_{12}$ capacitor-varistors. J Mater Sci: Mater Electron, 2013, 24, 1994
[55] Xiao M, Wang K Y, Chenyang X Q, et al. Nonlinear current-voltage behavior of $CaCu_3Ti_4O_{12}$ thin films derived from Sol-gel method. J Mater Sci: Mater Electron, 2014, 25, 2710
[56] Felix A A, Orlandi M O, Varela J A. Schottky-type grain boundaries in CCTO ceramics. Solid State Commun, 2011, 151, 1377
[57] https://www.creativesaftysupply.com
[58] Abdullah K A L, Termanini M D, Omar F A. Effect of impurities and temperature on electrical properties of ZnO-based varistors. Energy Procedia, 2012, 18, 867
[59] Russell H W. Principles of heat flow in porous insulators. J Am

Ceram Soc, 1935, 18, 1

[60] Onodera A, Takesada M, Kawatani K, et al. Dielectric properties and phase transition in $CaCu_3Ti_4O_{12}$ at high temperatures. Jpn J Appl Phys, 2008, 47, 7753

[61] Gorev M V, Flerov I N, Kartashev A V, et al. Investigation of the thermal expansion and heat capacity of the $CaCu_3Ti_4O_{12}$ ceramics. Phys Solid State, 2012, 54, 1785

[62] Lakhani V K, Modi K B. Effect of Al^{3+} substitution on the transport properties of copper ferrite. J Phys D, 2011, 44, 245403

Kunal B. Modi is currently a professor of physics at Saurashtra University, Rajkot, India. His research interests focus on the synthesis and characterization of spinel ferrites and $CaCu_3Ti_4O_{12}$ – based perovskites. Dr. Modi has published more than 120 research papers in internationally-reputed journals. Dr. Modi has received three national awards.